Single-Atom Control of Single-Molecule van der Waals Junctions with Semimetallic Transition Metal Dichalcogenides Electrodes

Zhixing Lu[1]‡, Songjun Hou[2]‡, Rongjian Lin[1], Jie Shi[1], Qingqing Wu[2], Shiqiang Zhao[1], Luchun Lin[1], Chun Tang[1], Yang Yang[1], Colin J. Lambert[2]*, Wenjing Hong[1]**

[1]State Key Laboratory of Physical Chemistry of Solid Surfaces, College of Chemistry and Chemical Engineering & Pen-Tung Sah Institute of Micro-Nano Science and Technology, IKKEM, Xiamen University, Xiamen 361005, China

[2]Department of Physics, Lancaster University, Lancaster LA1 4YB, United Kingdom.

Corresponding Authors:

*Yang Yang; Email: yangyang@xmu.edu.cn

*Colin J. Lambert; Email: c.lambert@lancaster.ac.uk

*Wenjing Hong; Email: whong@xmu.edu.cn

KEYWORDS. single-molecule junction, transition metal dichalcogenides, van der Waals interaction, break junction, charge transport

ABSTRACT. Electrodes play an essential role in controlling the electrode-molecule coupling. However, conventional metal electrodes require linkers to anchor the molecule. Van der Waals interaction offers a versatile strategy to connect the electrode and molecule without anchor groups. Except for graphene, the potential of other materials as electrodes to fabricate van der Waals molecular junctions remains unexplored. Herein, we utilize semimetallic transition metal dichalcogenides (TMDCs) 1T'-WTe_2 as electrodes to fabricate WTe_2/metallated tetraphenylporphyrin (M-TPP)/WTe_2 junctions via van der Waals interaction. Compared with chemically bonded Au/M-TPP/Au junctions, the conductance of these M-TPP van der Waals molecular junction is enhanced by ~736%. More importantly, WTe_2/M-TPP/WTe_2 junctions exhibit the tunable conductance from $10^{-3.29}$ G_0 to $10^{-4.44}$ G_0 (1.15 orders of magnitude) via single-atom control, recording the widest tunable range of conductance for M-TPP molecular junctions. Our work demonstrates the potential of two-dimensional TMDCs for constructing highly tunable and conductive molecular devices.

As an essential component of molecular devices, the electrodes determine the electrode-molecule coupling and the charge transport mechanism across the molecule[1,2]. Noble metals (e.g. Au, Ag, Pt) were widely used as electrodes for the single-molecule junction. Anchor groups are necessary to connect the molecule with metal electrodes and form covalent bonds, which requires organic synthesis and limits to some particular groups (e.g., -SH, -NH_2, -COOH)[3–7]. Van der Waals

interaction provides a versatile strategy to construct molecular junctions without anchor groups, which will greatly expand the choice of molecules. To date, only graphene electrodes have been used to fabricate van der Waals molecular junctions[8], which limited the development of these molecular devices.

Compared with graphene, transition metal dichalcogenides (TMDCs) have richer compositions and structures, along with the adjustable bandgap[9], which holds the potential to modulate the properties of molecular junctions through the electrodes[10]. Among these materials family, semimetallic TMDCs (e.g., 1T'-$MoTe_2$, 1T'-WTe_2) exhibit high conductivity and become promising electrode materials in two-dimensional electronic components[11–13]. Moreover, these layered two-dimensional semimetals stack by van der Waals interaction and the surface is free of the dangling bonds, which will not introduce the interface chemical bonds and thus suppress Fermi level pinning effect[14]. Therefore, utilizing these semimetallic TMDCs as electrodes to fabricate single-molecule junctions via van der Waals interaction provides a potential solution for optimizing the charge transport and functionality. Single-atom control of the molecule offers an opportunity to modulate the charge transport from the atomic level[15,16], but its effects on the charge transport through a van der Waals molecular junction remained unexplored.

Herein, we developed an approach to fabricate van der Waals interaction-based single-molecule junctions with semimetallic 1T'-WTe_2 electrodes, and investigated the charge transport of metallated tetraphenylporphyrin (M-TPP) molecules by an upgraded scanning tunneling microscope break junction (STM-BJ) (Figure 1A). By changing the metal center of M-TPP molecules (Figure 1B), the conductance of WTe_2/M-TPP/WTe_2 junctions can be tuned by ~1.15 orders of magnitude, from $10^{-3.29}$ G_0 (39.75 nS) to $10^{-4.44}$ G_0 (2.81 nS). Benefiting from the localized edge states of 1T'-WTe_2 electrodes and closer-lying frontier orbital, the more conduction

channels and the smaller contact resistance facilitate the charge transport across WTe_2/M-TPP/WTe_2 junctions, of which the conductance is comparable to, or even larger than M-TPP junction with Au electrodes through covalent bonding. This work demonstrated a novel method for constructing single-molecule junctions by semimetallic TMDCs electrodes, which holds the potential to improve the tunability and efficiency of charge transport for molecular devices.

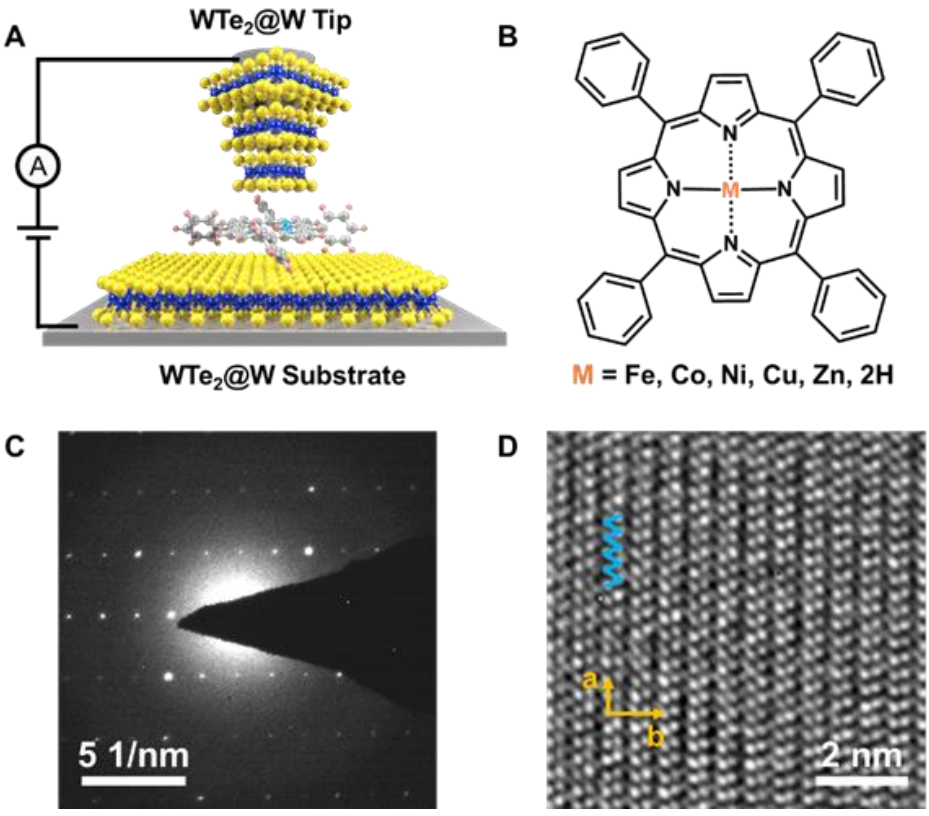

Figure 1. (A) Schematic of the single-molecule junction constructed by 1T'-WTe_2 electrodes. (B) The molecular structure of M-TPP. (C) SAED patterns of as-synthesized 1T'-WTe_2. (D) HRTEM image of as-synthesized 1T'-WTe_2.

To obtain the TMDCs electrodes for the single-molecule conductance measurement, tungsten was used as the precursor and template, and a two-step route was performed to synthesize WTe_2 tip and substrate, as detailed in the Methods. The Raman spectrum (Figure S1) exhibits five peaks at 88 cm^{-1}, 113 cm^{-1}, 131 cm^{-1}, 162 cm^{-1}, and 210 cm^{-1}, as contributed by the vibration modes of 1T' phase of WTe_2[17]. Scanning electron microscope (SEM) and transmission electron microscope (TEM) were utilized to investigate the morphology and crystal structure of as-synthesized WTe_2 electrodes. SEM and TEM (Figure S2) images revealed that both layer-by-layer stacked and vertically aligned WTe_2 nanosheets were grown on the surface of tungsten foil and wire, of which the exposed edge sites can enhance the electron transport efficiency of the as-prepared WTe_2 electrodes[12]. Selected-area electron diffraction (SAED) pattern (Figure 1C) taken at the nanosheet exhibited one set of rectangle-like diffraction points and matched well with [1 1 1] zone axis of 1T'-WTe_2. Moreover, high-resolution TEM (HRTEM) image (Figure 1D) showed clear zigzag W chains along the **a** axis, and the lattice parameters derived from the intensity line profiles were a = 3.5 Å and b = 6.2 Å, consistent with the previous reports[11,17,18]. These results suggest the high crystallinity and 1T' phase of as-synthesized WTe_2 electrodes.

To verify the feasibility of using 1T'-WTe_2 as electrodes for molecular junctions, metallated tetraphenylporphyrin (M-TPP) molecules (M=Fe, Co, Ni, Cu, Zn, 2H) were selected, and their charge transport properties were measured using the upgraded STM-BJ technique. Conductance measurements were carried out in a decane solution containing 0.1 mM of M-TPP molecules, and a bias of 100 mV was applied between the tip and substrate. Once a plateau of the molecular junction was monitored in the preset conductance range ($10^{-2.5}$~$10^{-5.5}$ G_0), the movement of the tip was kept for 100 ms and the conductance traces were recorded.

For comparison, we firstly used the traditional Au electrodes to construct M-TPP molecular junctions. At the constant stretching speed of 3 nm/s, the conductances of the M-TPP molecules decreased exponentially as the time increased, and no clear plateau was recorded (Figure S3). One-dimensional (1D) conductance histogram showed no obvious statistical peak of conductance (Figure S4). These results indicated that Au electrodes can hardly form stable Au/M-TPP/Au junctions without anchor groups like thiol (-SH) or methylthio (-SCH_3). We also performed the conductance measurements for M-TPP molecules on 1T'-WTe_2 substrate with Au tip, namely, the asymmetric electrodes pair. We found that only Fe-TPP, Co-TPP and TPP molecules could be captured, and the measured conductances were about $10^{-3.5}$~$10^{-4.3}$ G_0 (Figure S5 and S6).

In contrast, when we measured the molecules with the 1T'-WTe_2 substrate and 1T'-WTe_2 tip, the typical conductance traces (Figure 2A) showed clear conductance plateaus ranging from 10^{-3} G_0 to 10^{-5} G_0 for each M-TPP and TPP molecule, indicating the formation of WTe_2/M-TPP/WTe_2 junctions. 1D conductance histograms (Figure 2B) and 2D conductance-time histograms (Figure 2C) were constructed by overlapping thousands of individual conductance traces. By statistically analyzing the 1D conductance histograms, it is found that Fe-TPP, Co-TPP, Ni-TPP, Cu-TPP, Zn-TPP and TPP molecular junctions possess the peaks located at $10^{-3.29}$ G_0 (39.75 nS), $10^{-3.68}$ G_0 (16.19 nS), $10^{-4.19}$ G_0 (5.00 nS), $10^{-4.11}$ G_0 (6.02 nS), $10^{-4.44}$ G_0 (2.81 nS), and $10^{-4.05}$ G_0 (6.91 nS), respectively, which are summarized in Figure 2D and Table 1. The distinct conductance intensity clouds in 2D conductance-time histograms, of which the positions correspond with the peaks in 1D conductance histograms, indicate the formation of stable molecular junctions with these 1T'-WTe_2 electrodes. The conductances of M-TPP have been tuned by ~1.15 orders of magnitude by changing the metal centers, which records the widest tunable range of conductance for M-TPP molecular junctions reported so far[19,20]. Moreover, the conductances of M-TPP molecular

junctions fabricated with 1T'-WTe_2 electrodes are comparable to that with Au electrodes through covalent bonding[19–22]. For Fe-TPP[20] and Co-TPP[19], the conductances were even improved by ~413% and ~736% by using 1T'-WTe_2 electrodes (Figure 2D). It was also found that the conductance of WTe_2/M-TPP/WTe_2 junctions increased as the number of unpaired electrons in the metal center increased. The conductance of Fe-TPP with three unpaired electrons was ~2.45 times as large as that of Co-TPP with one unpaired electron, and ~14.13 times as large as that of Zn-TPP without unpaired electrons.

Moreover, we measured the conductance of M-TPP molecules with different concentrations, and investigated the formation probability of junctions therein[23]. As shown in Figure S7, the formation probability of WTe_2/M-TPP/WTe_2 junction is dependent on the concentration, while the conductance value is independent of the concentration, indicating that the measured conductance comes from a single probe molecule.

To further investigate the applicability of 1T'-WTe_2 electrodes in the fabrication of molecular junctions, we also tried to use these electrodes to measure the conductance of other molecules without anchor groups, such as oligo(phenylene-ethynylene) (OPE3), and phthalocyanine (Pc) (Figure S8). Clear plateau and distinct peaks were observed in the 2D and 1D conductance histogram, respectively, indicating that the molecular junctions were formed by using 1T'-WTe_2 electrodes. The conductance of OPE3 and Pc are $10^{-3.96}$ G_0 (8.49 nS) and $10^{-2.73}$ G_0 (144.31 nS) by Gaussian fitting of the peaks, respectively. These results indicate the versatility of these 1T'-WTe_2 electrodes in the fabrication of molecular junctions.

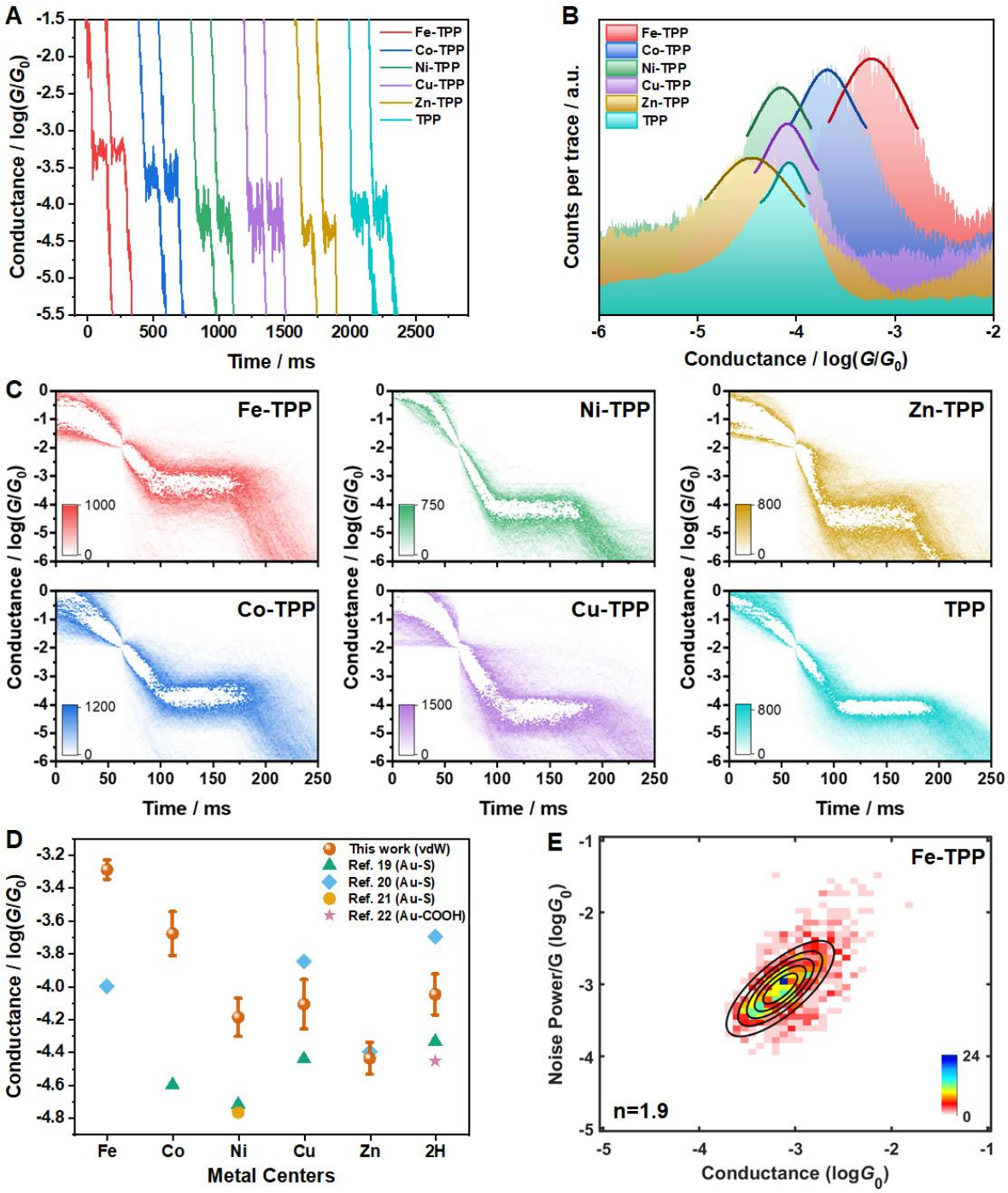

Figure 2. (A) Typical conductance traces versus time measured with M-TPP (M=Fe, Co, Ni, Cu, Zn) and TPP single-molecule junctions. (B) 1D conductance histograms for M-TPP (M=Fe, Co, Ni, Cu, Zn) and TPP single-molecule junctions. (C) 2D conductance-time histograms of the M-

TPP (M=Fe, Co, Ni, Cu, Zn) and TPP single-molecule junctions. (D) The conductances of M-TPP single-molecule junctions with WTe_2 electrodes and Au electrodes. (E) 2D histogram of normalized flicker noise power versus average conductance for Fe-TPP single-molecule junctions with WTe_2 electrodes.

Flicker noise analysis was recently developed to distinguish the dominant charge transport pathway through the single-molecule junction.[24] The value of the noise power reveals the mechanism of charge transport that $G^{1.0}$ represents a complete through-bond transport, while $G^{2.0}$ represents a complete through-space transport.[25] To perform the flicker noise analysis, the tip was stopped at the position where WTe_2/M-TPP/WTe_2 junction was formed and held for 150 ms for collecting the conductance-time curves, from which the noise spectrum was extracted by Fourier transform. The flicker noise power spectral density (PSD) was obtained by integrating the noise spectrum 100 to 1000 Hz and normalized by the average conductance. Figure 2E and Figure S9 showed the 2D histograms of normalized flicker noise power versus average conductance, which were fitted by 2D Gaussian distribution as the plotted black contour lines. The noise power of M-TPP evolved as 1.9 (Fe-TPP), 1.8 (Co-TPP), 1.7 (Ni-TPP), 2.0 (Cu-TPP), 1.9 (Zn-TPP), and 1.9 (TPP), respectively, indicating the charge transport from WTe_2 electrode to M-TPP molecules is dominated by the through-space pathway, which further verifies no chemical bonding between the electrode and molecule.

The current-voltage (*I-V*) characteristics provided a sight into the electronic structures of the single-molecule junction, including the electrode-molecule coupling (Γ) and the energy level alignment (ε). Herein, *I-V* characteristics were measured with a bias ranging from -0.5 V to 0.5 V when the corresponding plateau emerged at the measured conductance traces. 2D *I-V* histograms are constructed by collecting more than 1000 *I-V* curves, as shown in Figure 3A and Figure S10.

2D conductance-voltage (*G-V*) histograms of WTe_2/M-TPP/WTe_2 junctions are shown in Figure 3B and Figure S11. The Gaussian fitted *I–V* and *G-V* curves are symmetric and no obvious rectification was observed. The energy level corresponding to unpaired electrons of M-TPP molecules are located close to Fermi energy, therefore they introduce a nearby resonance in the transmission curves. To obtain the parameters of electronic structure, the single-transmission-resonance model was used to analyze the *I-V* curves. The current through the single-molecule junction can be given by Landauer−Büttiker formula[26–28].

$$I(V) = \frac{2e}{h}\int_{-\infty}^{+\infty} dE \cdot \tau(E)[f(E - \frac{eV}{2}) - f\left(E + \frac{eV}{2}\right)] \quad (1)$$

$$\tau(E) = \frac{4\Gamma_s\Gamma_t}{(\Gamma_s+\Gamma_t)^2+(E-\varepsilon)^2} \quad (2)$$

where τ is the transmission probability, ε is the energy level alignment, which means the energy difference between the Fermi level and the molecular orbital energy level, and Γ_s (Γ_t) is the electronic coupling energy between the molecule and the substrate (tip) electrode. As the electrodes are symmetric, $\Gamma_s=\Gamma_t= 0.5\Gamma$, and the equation can be simplified as

$$I(V) = \frac{8e}{h}\frac{\Gamma_s\Gamma_t}{\Gamma_s+\Gamma_t}\left[\tan^{-1}(\frac{eV\times\Gamma_s/\Gamma-\varepsilon}{\Gamma}) + \tan^{-1}(\frac{eV\times\Gamma_t/\Gamma+\varepsilon}{\Gamma})\right] \quad (3)$$

Using the equation (3), Γ and ε can be extracted from the *I-V* curves, as shown in Figure 3C and Figure S12. The values of Γ and ε are summarized in Figure 3D and Table 1. Compared with chemically bonded M-TPP single-molecule junctions reported in the previous study[21], the electronic coupling of WTe_2/Ni-TPP/WTe_2 junction (Γ~4.807 meV) is much smaller than that of Au/Ni-TPP/Au junctions (Γ~13 meV), while the energy level alignment of WTe_2/Ni-TPP/WTe_2 (ε~0.328 eV) is smaller than that of Au/Ni-TPP/Au junctions (ε~0.85 eV). And the value of Γ is

much smaller than ε for WTe_2/M-TPP/WTe_2 junctions. These results confirm that a weak coupling between the WTe_2 electrode and M-TPP molecule[1,2], and the origin of the increased conductance of WTe_2/M-TPP/WTe_2 junctions is closer-lying frontier orbital. It is also observed that the electronic coupling is positively correlated with the number of unpaired electrons in the metal center, which follows the same trend as the conductance (Fe-TPP>Co-TPP>TPP>Cu-TPP>Ni-TPP>Zn-TPP).

To characterize the barrier between the electrode and molecule, we extracted the transition voltage spectroscopy (TVS) from the Fowler–Nordheim (F-N) plot of $\ln(I/V^2)$ versus $1/V$ [29–31]. In TVS curves, the transition voltage (V_{trans}, the minimum value of TVS) is proportional to the energy offset between the electrode Fermi energy (E_F) and the molecular frontier orbital[32]. Thus, it can be used as an indicator to predict contact resistance. Figure 3E and Figure S13 show the F–N plots for the fitted *I–V* curves of WTe_2/M-TPP/WTe_2 junctions. As the reference, the TVS of WTe_2 electrode in the pure decane solution was measured, and no V_{trans} was observed in the scanning bias range of ±0.5 V (Figure S14). For WTe_2/M-TPP/WTe_2 junctions, the obvious inflection behavior was observed in the TVS, as divided into blue and yellow regimes. The values of V_{trans} are summarized in Figure 3F and Table 1. The low V_{trans} (<1.0 V) value demonstrated the formation of molecular junctions rather than air tunneling junctions[30]. It was also found that all the V_{trans} values therein are much smaller than most molecular junctions formed by Au electrodes (0.6~1.0 V)[30,31,33], which further verified the feasibility of reducing the tunneling barrier by using WTe_2 as electrodes.

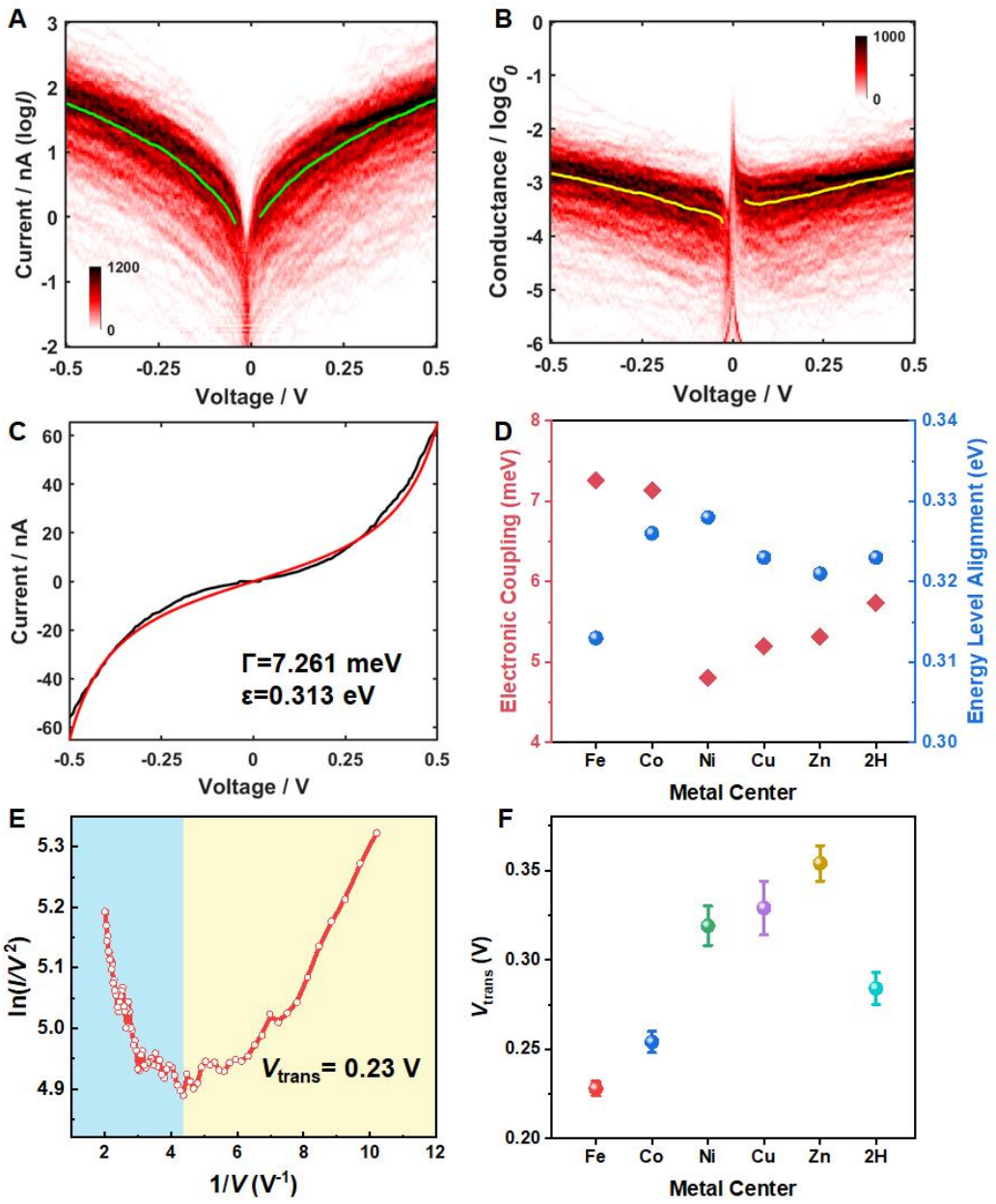

Figure 3. (A) 2D *I-V* histogram of WTe_2/Fe-TPP/WTe_2 junctions. The green line represents the Gaussian fitted curve. (B) 2D *G-V* histogram of WTe_2/Fe-TPP/WTe_2 junctions. The yellow line represents the Gaussian fitted curve. (C) Gaussian fitted *I-V* curve extracted from Figure 3A (black line) and the fitted *I-V* curves according to the single-level model (red line). (D) The electrode-molecule coupling (Γ) and the energy level alignment of WTe_2/M-TPP/WTe_2 junctions. (E)

Fowler-Nordheim plot of WTe_2/Fe-TPP/WTe_2 junctions. (F) Transition voltage (V_{trans}) of WTe_2/M-TPP/WTe_2 junctions.

Table 1. The single-molecule conductances and electronic structure parameters of WTe_2/M-TPP/WTe_2 junctions. The data includes the electrode-molecule coupling (Γ), the energy level alignment (ε), the transition voltage (V_{trans}), and the number of unpaired electrons (n_{ue}) in the metal center.

Molecule	G / logG_0	**Γ / meV**	**ε / eV**	V_{trans} / V	n_{ue}
Fe-TPP	-3.29	7.261	0.313	0.23	3
Co-TPP	-3.68	7.136	0.326	0.25	1
Ni-TPP	-4.19	4.807	0.328	0.32	0
Cu-TPP	-4.11	5.196	0.323	0.33	1
Zn-TPP	-4.44	5.315	0.321	0.31	0
TPP	-4.05	5.734	0.323	0.28	0

To further elucidate the transport properties of WTe_2/M-TPP/WTe_2 junctions with the different metal centers, we calculated their cross-plane transmission functions, *T(E)*, by combining the density functional theory (DFT) package SIESTA[34] with the quantum transport code Gollum[35] (see details in Methods). Transport properties were investigated by embedding TPP molecules between two 1T'-WTe_2 electrodes (Figure 4A). To decrease the influence of finite-size effects, periodic boundary conditions were used in the two directions perpendicular to the direction of the current flow. An optimal distance of 4.4 Å between the metal center of M-TPP and the electrode was determined by evaluating the binding energy as a function of distance (Figure S15 and S16). To demonstrate whether the meso-phenyl side groups affects the conductance trend, we performed

the charge transport calculation for Co-TPP and Cu-TPP/WTe_2 junctions in the presence of meso-phenyl side groups (Figure S17A). As shown in Figure S17B and C, Co-TPP shows higher conductance than that of Cu-TPP in the energy range close to DFT-predicted Fermi energy, qualitatively agreeing with our results without meso-phenyl side groups (Figure S18). Therefore, the meso-phenyl side groups were replaced by hydrogen atoms to simplify the calculation and reduce the considerable computational overhead.

Our modeling indicated that electrodes bind to the porphyrin core and that current flows are perpendicular to the plane of the porphyrin core. It was found that numerical convergence for WTe_2 system is difficult to achieve compared to the conventional single-molecule junctions with Au electrodes, due to the longer screening length in the semimetallic WTe_2. The corresponding total conductances are presented in Figure 4, and the spin polarized conductances are shown in Figure S18. In the case of M=Fe, Co, the spin-up conductance is much higher than the spin-down conductance near Fermi energy resulting in higher conductance for Fe-TPP and Co-TPP (Figure 4B and Figure S18A, B). On the other hand, for M=Ni, Cu, Zn, 2H, both the spin-up and spin-down conductances show very small values in the energy range close to the DFT-predicted Fermi energy (Figure 4B and Figure S18C-F). To show that this spin polarization is ascribed to the intrinsic property of the molecules, the M-TPP molecules were placed between two flat Au electrodes (Figure 4C) and their transport properties were computed (Figure 4D and Figure S19). As shown in Figure 4D, in the presence of Au electrodes, Fe-TPP and Co-TPP also show a higher conductance compared to the other members in the M-TPP family due to the spin polarization in the single-molecule junction. This spin polarization is induced by the metal center of M-TPP molecule as demonstrated by the partial density of states (PDOS) (Figure S20), where 3d orbitals play a significant role. In WTe_2/Co-TPP/WTe_2 junction, the energy offsets between the electrode

Fermi energy (E_F) and singly occupied orbital is around 0.31 eV, which is smaller than that (0.37 eV) of the WTe_2/Co-TPP/WTe_2 junction (Figure S21). A smaller energy offset implies a lower energy barrier in the WTe_2/Co-TPP/WTe_2 junction, which qualitatively supports the conclusion based on the TVS study.

In the case of WTe_2, we find the local density of states (LDOS) near Fermi energy is localized at the electrode surfaces, signifying the presence of electronic edge states (Figure 4A). The LDOS is mainly localized on the W atoms close to the gap, which increases the conduction channels close to Fermi energy and boosts the transmission probability through the junction. In contrast, for Au electrodes, the LDOS near Fermi energy is distributed over the whole electrode (Figure 4C), which results in a lower transmission probability compared with the WTe_2 electrodes. Therefore, as shown in Figure 4B and 4D, the conductance of WTe_2/M-TPP/WTe_2 junction with a larger electrode gap (8.8 Å) is higher than Au/M-TPP/Au junction with a smaller gap (7 Å). These calculations demonstrate that electrodes not only maintain the spin polarization of M-TPP molecules, but also reduce the contact resistance due to the localized edge states which are located close to Fermi energy, resulting in the enhanced charge transport across the junction.

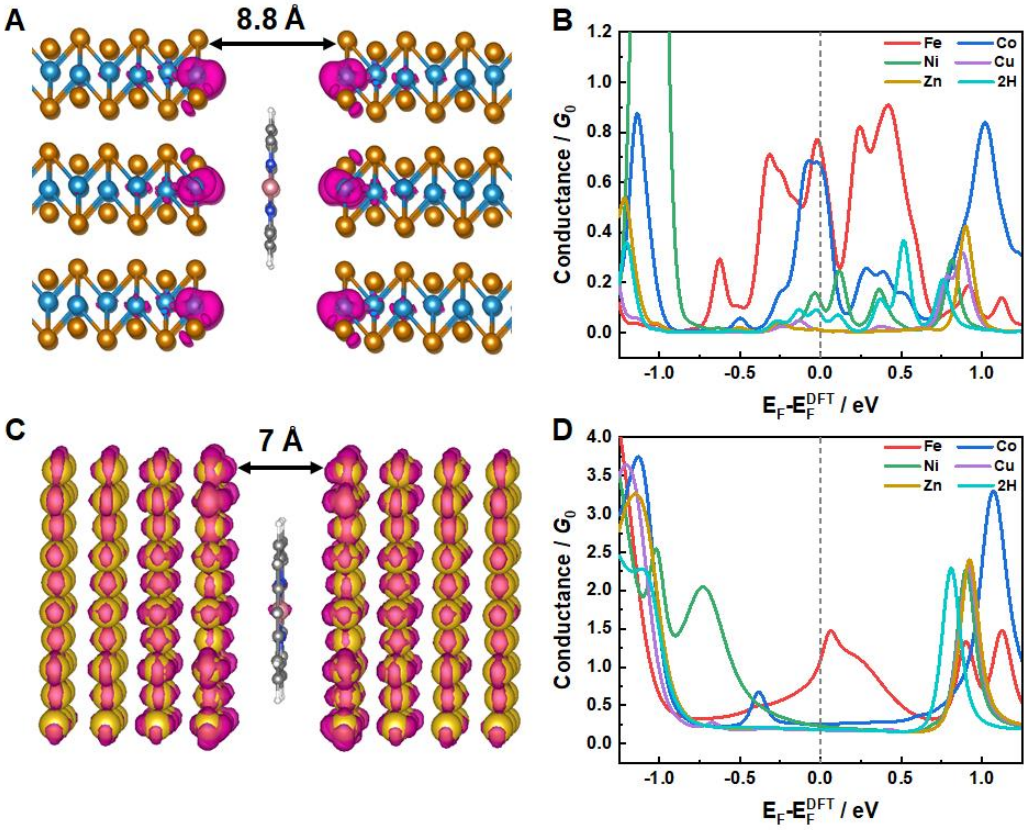

Figure 4. (A) Model of the WTe_2/M-TPP/WTe_2 junction for calculations, where M-TPP is sandwiched between two WTe_2 electrodes. LDOS of WTe_2/M-TPP/WTe_2 with magenta color in the energy window from -0.5 to 0.5 eV. W and Te atoms are represented by blue and yellow spheres, respectively. The side groups of the M-TPP are omitted and replaced by hydrogens for simplification. (B) The total conductances for WTe_2/M-TPP/WTe_2 junctions. (C) Model of the Au/M-TPP/Au single-molecule junction for calculations, where M-TPP is sandwiched between two Au electrodes. LDOS of Au/M-TPP/WTe_2 with magenta color in the energy window from -0.5 to 0.5 eV. (D) The total conductances for Au/M-TPP/Au single-molecule junctions.

In summary, we developed a versatile strategy to fabricate highly tunable and conductive molecular devices by utilizing semimetallic 1T'-WTe_2 as electrodes. Diverse single-molecule junctions based on van der Waals interactions, such as OPE3, Pc and M-TPP molecules, were constructed using 1T'-WTe_2 as electrodes, and their charge transport properties are investigated using a combination of the STM-BJ technique and DFT-based quantum transport calculations. Benefiting from the presence of localized edge states localized on W surface atoms, 1T'-WTe_2 electrodes facilitate the charge transfer at the electrode-molecule interface and reduce the contact resistance, which dramatically improves the conductance of M-TPP single-molecule junctions by ~736%. With these 1T'-WTe_2 electrodes, the conductance of M-TPP single-molecule junctions was modulated by ~1.15 orders of magnitude by altering the metal center, which achieved the widest tunable range of M-TPP single-molecule junctions. The combined PSD analysis and DFT calculations demonstrated that the through-space mechanism accounts for the charge transport through the WTe_2/M-TPP/WTe_2 junctions, and the charge transport properties showed a positive correlation to the number of unpaired electrons in the metal center. These findings suggest that the employment of TMDCs electrodes opens a new avenue to construct single-molecule junctions beyond the conventional metallic electrodes, and achieve higher conductance and wider tunable conductance range in the charge transport of M-TPP molecules by the single-atom control. Our work reveals the potential of using TMDCs as electrodes to fabricate highly tunable and conductive molecular devices through van der Waals interaction, and provides a facile and versatile approach for designing functional molecular devices with tunable conductance.

ASSOCIATED CONTENT

Supporting Information

The Supporting Information is available free of charge on the ACS Publications website.

Materials and methods, characterization of as-synthesized 1T'-WTe_2, the conductance measurement of M-TPP molecules, flicker noise analysis, analysis of I-V characteristics, and theoretical calculations (PDF)

AUTHOR INFORMATION

Corresponding Author

*Yang Yang; Email: yangyang@xmu.edu.cn

*Colin J. Lambert; Email: c.lambert@lancaster.ac.uk

*Wenjing Hong; Email: whong@xmu.edu.cn

Author Contributions

‡Z.L. and S.H. contributed equally to this work. Z.L., Y.Y., and W.H. conceived the ideas. W.H., Y.Y. and C.J.L. supervised this project. Z.L., R.L., J.S. and S.Z. carried out the break junction experiments and analyzed the results. C.T. and L.L. provided the code to analyze the data. S.H., Q.W. and C.J.L. performed the theoretical calculations. Z.L., S.H., Y.Y., W.H. and C.J.L. wrote the manuscript with input from all authors. All the authors discussed the results and commented on the manuscript.

Notes

The authors declare no competing financial interest.

ACKNOWLEDGMENT

We acknowledge the support from the National Natural Science Foundation of China (T2222002, 21973079, 22032004, 21991130), the National Postdoctoral Program for Innovative Talent (BX20180179), the Natural Science Foundation of Fujian Province (2021J06008), the UK EPSRC Grants (EP/M014452/1, EP/P027156/1, EP/N03337X/1).

REFERENCES

(1) Jia, C.; Guo, X. Molecule–Electrode Interfaces in Molecular Electronic Devices. *Chem. Soc. Rev.* **2013**, *42* (13), 5642–5660.

(2) Xiang, D.; Wang, X.; Jia, C.; Lee, T.; Guo, X. Molecular-Scale Electronics: From Concept to Function. *Chem. Rev.* **2016**, *116* (7), 4318–4440.

(3) Nakazumi, T.; Kaneko, S.; Kiguchi, M. Electron Transport Properties of Au, Ag, and Cu Atomic Contacts in a Hydrogen Environment. *J. Phys. Chem. C* **2014**, *118* (14), 7489–7493.

(4) Kim, T.; Vázquez, H.; Hybertsen, M. S.; Venkataraman, L. Conductance of Molecular Junctions Formed with Silver Electrodes. *Nano Lett.* **2013**, *13* (7), 3358–3364.

(5) Arroyo, C. R.; Leary, E.; Castellanos-Gómez, A.; Rubio-Bollinger, G.; González, M. T.; Agraït, N. Influence of Binding Groups on Molecular Junction Formation. *J. Am. Chem. Soc.* **2011**, *133* (36), 14313–14319.

(6) Smit, R. H. M.; Noat, Y.; Untiedt, C.; Lang, N. D.; Van Hemert, M. C.; Van Ruitenbeek, J. M. Measurement of the Conductance of a Hydrogen Molecule. *Nature* **2002**, *419* (6910), 906–909.

(7) Li, L.; Low, J. Z.; Wilhelm, J.; Liao, G.; Gunasekaran, S.; Prindle, C. R.; Starr, R. L.; Golze, D.; Nuckolls, C.; Steigerwald, M. L.; Evers, F.; Campos, L. M.; Yin, X.; Venkataraman, L. Highly Conducting Single-Molecule Topological Insulators Based on Mono- and Di-Radical Cations. *Nat. Chem.* **2022**, *14* (9), 1061–1067.

(8) Zhao, S.; Wu, Q.; Pi, J.; Liu, J.; Zheng, J.; Hou, S.; Wei, J.; Li, R.; Sadeghi, H.; Yang, Y.; Yang, Y.; Shi, J.; Chen, Z.; Xiao, Z.; Xiao, Z.; Lambert, C.; Hong, W.; Hong, W. Cross-Plane Transport in a Single-Molecule Two-Dimensional van Der Waals Heterojunction. *Sci. Adv.* **2020**, *6* (22), eaba6714.

(9) Chhowalla, M.; Shin, H. S.; Eda, G.; Li, L. J.; Loh, K. P.; Zhang, H. The Chemistry of Two-Dimensional Layered Transition Metal Dichalcogenide Nanosheets. *Nat. Chem.* **2013**, *5* (4), 263–275.

(10) Shin, J.; Yang, S.; Jang, Y.; Eo, J. S.; Kim, T. W.; Lee, T.; Lee, C. H.; Wang, G. Tunable Rectification in a Molecular Heterojunction with Two-Dimensional Semiconductors. *Nat. Commun.* **2020**, *11* (1), 1412.

(11) Soares, D. M.; Singh, G. Superior Electrochemical Performance of Layered WTe2 as Potassium-Ion Battery Electrode. *Nanotechnology* **2020**, *31* (45), 455406.

(12) Shi, Y.; Kahn, J.; Niu, B.; Fei, Z.; Sun, B.; Cai, X.; Francisco, B. A.; Wu, D.; Shen, Z. X.; Xu, X.; Cobden, D. H.; Cui, Y. T. Imaging Quantum Spin Hall Edges in Monolayer WTe 2. *Sci. Adv.* **2019**, *5* (2), eaat8799.

(13) Liu, Y.; Stradins, P.; Wei, S. H. Van Der Waals Metal-Semiconductor Junction: Weak Fermi Level Pinning Enables Effective Tuning of Schottky Barrier. *Sci. Adv.* **2016**, *2* (4), e160006.

(14) Liu, Y.; Guo, J.; Zhu, E.; Liao, L.; Lee, S. J.; Ding, M.; Shakir, I.; Gambin, V.; Huang, Y.; Duan, X. Approaching the Schottky-Mott Limit in van Der Waals Metal-Semiconductor Junctions. *Nature* **2018**, *557* (7707), 696–700.

(15) Meng, L.; Xin, N.; Wang, J.; Xu, J.; Ren, S.; Yan, Z.; Zhang, M.; Shen, C.; Zhang, G.; Guo, X.; Meng, S. Atomically Precise Engineering of Single-Molecule Stereoelectronic Effect. *Angew. Chemie - Int. Ed.* **2021**, *60* (22), 12274–12278.

(16) Tang, C.; Huang, L.; Sangtarash, S.; Noori, M.; Sadeghi, H.; Xia, H.; Hong, W. Reversible Switching between Destructive and Constructive Quantum Interference Using Atomically Precise Chemical Gating of Single-Molecule Junctions. *J. Am. Chem. Soc.* **2021**, *143* (25), 9385–9392.

(17) Chen, K.; Chen, Z.; Wan, X.; Zheng, Z.; Xie, F.; Chen, W.; Gui, X.; Chen, H.; Xie, W.; Xu, J. A Simple Method for Synthesis of High-Quality Millimeter-Scale 1T′ Transition-Metal Telluride and Near-Field Nanooptical Properties. *Adv. Mater.* **2017**, *29* (38), 1700704.

(18) Kwak, J.; Jo, Y.; Song, S.; Kim, J. H.; Kim, S. Y.; Lee, J. U.; Lee, S.; Park, J.; Kim, K.; Lee, G. Do; Yoo, J. W.; Kim, S. Y.; Kong, Y. M.; Lee, G. H.; Lee, W. G.; Park, J.; Xu, X.; Cheong, H.; Yoon, E.; Lee, Z.; Kwon, S. Y. Single-Crystalline Nanobelts Composed of Transition Metal Ditellurides. *Adv. Mater.* **2018**, *30* (30), 1707260.

(19) Liu, Z. F.; Wei, S.; Yoon, H.; Adak, O.; Ponce, I.; Jiang, Y.; Jang, W. D.; Campos, L. M.; Venkataraman, L.; Neaton, J. B. Control of Single-Molecule Junction Conductance of Porphyrins via a Transition-Metal Center. *Nano Lett.* **2014**, *14* (9), 5365–5370.

(20) Seng, J. W.; Tong, L.; Peng, X. Q.; Chang, W. Y.; Xie, W.; Wang, Y. H.; Zheng, J. F.; Shao, Y.; Chen, J. Z.; Jin, S.; Zhou, X. S. Influence of a Coordinated Metal Center on Charge Transport through a Series of Porphyrin Molecular Junctions. *J. Phys. Chem. C* **2022**, *126* (2), 1168–1175.

(21) Fujii, S.; Marqués-González, S.; Shin, J. Y.; Shinokubo, H.; Masuda, T.; Nishino, T.; Arasu, N. P.; Vázquez, H.; Kiguchi, M. Highly-Conducting Molecular Circuits Based on Antiaromaticity. *Nat. Commun.* **2017**, *8*, 15984.

(22) Li, Z.; Smeu, M.; Ratner, M. A.; Borguet, E. Effect of Anchoring Groups on Single Molecule Charge Transport through Porphyrins. *J. Phys. Chem. C* **2013**, *117* (29), 14890–14898.

(23) Zeng, B. F.; Zou, Y. L.; Wang, G.; Hong, W.; Tian, Z. Q.; Yang, Y. Quantitative Studies of Single-Molecule Chemistry Using Conductance Measurement. *Nano Today* **2022**, *47*, 101660.

(24) Garner, M. H.; Li, H.; Chen, Y.; Su, T. A.; Shangguan, Z.; Paley, D. W.; Liu, T.; Ng, F.; Li, H.; Xiao, S.; Nuckolls, C.; Venkataraman, L.; Solomon, G. C. Comprehensive Suppression of Single-Molecule Conductance Using Destructive σ-Interference. *Nature* **2018**, *558* (7710), 416–419.

(25) Adak, O.; Rosenthal, E.; Meisner, J.; Andrade, E. F.; Pasupathy, A. N.; Nuckolls, C.; Hybertsen, M. S.; Venkataraman, L. Flicker Noise as a Probe of Electronic Interaction at Metal-Single Molecule Interfaces. *Nano Lett.* **2015**, *15* (6), 4143–4149.

(26) Xie, Z.; Baldea, I.; Frisbie, C. D. Energy Level Alignment in Molecular Tunnel Junctions by Transport and Spectroscopy: Self-Consistency for the Case of Alkyl Thiols and Dithiols on Ag, Au, and Pt Electrodes. *J. Am. Chem. Soc.* **2019**, *141* (45), 18182–18192.

(27) Isshiki, Y.; Fujii, S.; Nishino, T.; Kiguchi, M. Fluctuation in Interface and Electronic Structure of Single-Molecule Junctions Investigated by Current versus Bias Voltage Characteristics. *J. Am. Chem. Soc.* **2018**, *140* (10), 3760–3767.

(28) Kim, Y.; Pietsch, T.; Erbe, A.; Belzig, W.; Scheer, E. Benzenedithiol: A Broad-Range Single-Channel Molecular Conductor. *Nano Lett.* **2011**, *11* (9), 3734–3738.

(29) Wang, Z.; Dong, H.; Li, T.; Hviid, R.; Zou, Y.; Wei, Z.; Fu, X.; Wang, E.; Zhen, Y.; Nørgaard, K.; Laursen, B. W.; Hu, W. Role of Redox Centre in Charge Transport Investigated by Novel Self-Assembled Conjugated Polymer Molecular Junctions. *Nat. Commun.* **2015**, *6*, 7478.

(30) Guo, S.; Hihath, J.; Díez-Pérez, I.; Tao, N. Measurement and Statistical Analysis of Single-Molecule Current-Voltage Characteristics, Transition Voltage Spectroscopy, and Tunneling Barrier Height. *J. Am. Chem. Soc.* **2011**, *133* (47), 19189–19197.

(31) Beebe, J. M.; Kim, B. S.; Frisbei, C. D.; Kushmerick, J. G. Measuring Relative Barrier Heights in Molecular Electronic Junctions with Transition Voltage Spectroscopy. *ACS Nano* **2008**, *2* (5), 827–832.

(32) Beebe, J. M.; Kim, B.; Gadzuk, J. W.; Frisbie, C. D.; Kushmerick, J. G. Transition from Direct Tunneling to Field Emission in Metal-Molecule-Metal Junctions. *Phys. Rev. Lett.* **2006**, *97* (2), 026801.

(33) Yang, Y.; Liu, J.; Feng, S.; Wen, H.; Tian, J.; Zheng, J.; Schöllhorn, B.; Amatore, C.; Chen, Z.; Tian, Z. Unexpected Current–Voltage Characteristics of Mechanically Modulated Atomic Contacts with the Presence of Molecular Junctions in an Electrochemically Assisted–MCBJ. *Nano Res.* **2016**, *9* (2), 560–570.

(34) Soler, J. M.; Artacho, E.; Gale, J. D.; García, A.; Junquera, J.; Ordejón, P.; Sánchez-Portal, D. The SIESTA Method for Ab Initio Order-N Materials Simulation. *J. Phys. Condens. Matter* **2002**, *14* (11), 2745–2779.

(35) Ferrer, J.; Lambert, C. J.; García-Suárez, V. M.; Manrique, D. Z.; Visontai, D.; Oroszlany, L.; Rodríguez-Ferradás, R.; Grace, I.; Bailey, S. W. D.; Gillemot, K.; Sadeghi, H.; Algharagholy, L. A. GOLLUM: A next-Generation Simulation Tool for Electron, Thermal and Spin Transport. *New J. Phys.* **2014**, *16*, 093029.

Table of Contents